Two-photon exchange effects in $e^+e^- \to \pi^+\pi^-$ and timelike pion electromagnetic form factor

Hong-Yu Chen and Hai-Qing Zhou*
School of Physics, Southeast University, NanJing 211189, China

(Received 15 June 2018; published 5 September 2018)

The two-photon-exchange (TPE) effects in the process $e^+e^- \to \pi^+\pi^-$ at large momentum transfer are discussed within the perturbative QCD (pQCD). The contributions from the twist-2 and twist-3 distribution amplitudes (DAs) of the pion are considered in the estimation. Different from the results under the one-photon-exchange (OPE) approximation, the TPE effects result in an asymmetry of the differential cross section on the scattering angle. The precise measurement of this asymmetry by the further experiment is a precise test of pQCD at large momentum transfer. The timelike electromagnetic form factor of the pion at the leading order (LO) of pQCD is rediscussed, and the comparison of our results with those in the references is presented. Our results show that the contributions from the twist-2 and twist-3 DAs in the LO of pQCD are much smaller than the experimental data at $Q^2 = 14.2, 17.4\ \mathrm{GeV}^2$, which is very different from the conclusion given in the references.

DOI: 10.1103/PhysRevD.98.054003

I. INTRODUCTION

The pion and the proton are the most elemental bound states due to the strong interaction. The knowledge on their structures is important to test our understanding of QCD. The electromagnetic (EM) form factor is one of the most simple and naive nonperturbative quantity reflecting the structures of these bound states.

In 2000, the measurements of the ratio of the EM form factors of the proton by the polarized method [1,2] gave very different results from those given by the Rosenbluth method [3,4]. This suggests the extraction of the EM form factors from the experimental data is a nontrivial problem. The two-photon-exchange (TPE) effects in the unpolarized ep scattering are expected to explain the discrepancy between the results from the polarized method and Rosenbluth method. Many theoretical methods have been used to estimate the TPE effects, such as the hadronic model [5–8], GPD method [9,10], phenomenological parametrizations [11,12], dispersion relation approach [13–18], pQCD calculations [19,20], and SCEF method [21]. The recent experimental results on the $R^{2\gamma} \equiv \sigma_{e^+p\to e^+p}/\sigma_{e^+p\to e^-p}$ [22] which measures the TPE effect directly shows the estimation by the most recent calculation [18] does not match the experimental data very well. All these mean our understanding on the TPE effects in the ep scattering still needs to be improved in both its theoretical and experimental aspects.

The TPE effects in the other processes also are interesting and are discussed in the references; these include, e.g., $e^+e^- \to p\bar{p}$ [23], $e\pi$ scattering [24,25] and unpolarized μp scattering [26–29]. In the literature, the TPE effects in the process $e^+e^- \to \pi^+\pi^-$ are usually ignored since the TPE effects will not affect the total cross section or the timelike EM form factor of the pion, while the TPE effects still play their role in the angle dependence of the differential cross section. The EM form factor of the pion in the spacelike region at high momentum transfer has played an important role in the test of pQCD factorization [30–32], while the experimental measurement of the EM form factor of the pion in the spacelike region is not a trivial problem since there is no pion target. The study of the EM form factor of the pion in the timelike region is another window to test the pQCD factorization [33–36]. The study of the TPE effects in this process also play a similar role to test the pQCD factorization and to help us understand the TPE effects. In this work, we estimate this effect and we also clarify some discussion on the timelike EM form factor of the pion at the leading order (LO) of pQCD given in the literature. We arrange our work as follows: in Sec. II, we give a simple introduction on the cross section of $e^+e^- \to \pi^+\pi^-$ and the timelike EM form factor of the pion by pQCD under the one-photon-exchange (OPE) approximation; in Sec. III we discuss the TPE effects in this process; in Sec. IV, we discuss the input used in our practical estimation; and in Sec. V, we give the numerical results and our conclusion.

*zhouhq@seu.edu.cn

II. $e^+e^- \to \pi^+\pi^-$ VIA ONE-PHOTON-EXCHANGE

In the OPE approximation, the process $e^+e^- \to \pi^+\pi^-$ can be described by the diagram shown in Fig. 1, and the corresponding amplitude can be expressed as

$$\mathcal{M}^{1\gamma} = [\bar{u}(-p_2, m_e)(-ie\gamma^\mu)u(p_1, m_e)]D_{\mu\nu}(q) \times [-ie(p_4 - p_3)^\nu F_\pi(s)], \quad (1)$$

where p_1, p_2, p_3, and p_4 are the momenta of the initial electron, initial antielectron, final π^- and π^+, $D_{\mu\nu}(q)$ is the photon propagator, $q = p_1 + p_2 = p_3 + p_4$, $Q^2 = q^2$, and $F_\pi(Q^2)$ is the timelike EM form factor of the pion which is defined as

$$\langle \pi^+\pi^-|j_\mu(0)|0\rangle \equiv -(p_4 - p_3)_\mu F_\pi(Q^2), \quad (2)$$

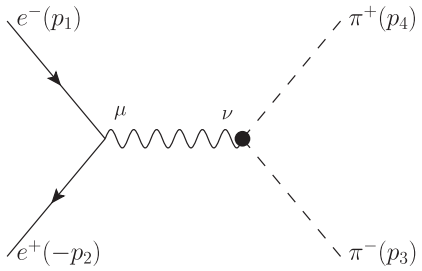

FIG. 1. Diagram for $e^+e^- \to \pi^+\pi^-$ with one-photon exchange (OPE).

with $j_\mu = \sum e_i\bar{q}_i\gamma_\mu q_i$, q_i the quark fields, i the flavor indexes of the quarks, and e_i the corresponding electric charge (-1 for electron).

By Eq. (1), the unpolarized differential cross section can be expressed as

$$d\sigma_{un}^{1\gamma} = \frac{1}{2}e^2F_\pi(Q^2)F_\pi^*(Q^2)\sin^2\theta, \quad (3)$$

where θ is the angle between the three momenta of the initial electron($\mathbf{p}_1$) and final $\pi^-(\mathbf{p}_3)$ in the center frame, $e = -|e| = -\sqrt{4\pi\alpha_{\rm QED}}$.

In the large momentum transfer region, the perturbative QCD (pQCD) can be applied to estimate the electromagnetic form factor $F_\pi(Q^2)$ [37]. In the LO of the strong interaction coupling α_s, the corresponding Feynman diagrams are shown as Fig. 2 and the corresponding contribution can be expressed as

$$F_\pi^{(a)}(Q^2) = \frac{(p_4 - p_3)_\nu}{-ie(p_4 - p_3)^2}\int_0^1 dxdy\int_{-\infty}^{\infty} d^2\mathbf{b}_1 d^2\mathbf{b}_2 \times \int_{-\infty}^{\infty}\frac{d^2\mathbf{k}_{\perp 1}}{(2\pi)^2}\frac{d^2\mathbf{k}_{\perp 2}}{(2\pi)^2}e^{-i\mathbf{b}_1\cdot\mathbf{k}_{\perp 1} - i\mathbf{b}_2\cdot\mathbf{k}_{\perp 2}} \times e^{-S(x,y,b_1,b_2,Q)}S_t(x)S_t(y)T_H^{\nu,(a)}, \quad (4)$$

where $b_1 = |\mathbf{b}_1|, b_2 = |\mathbf{b}_2|$, $S(x, y, b_1, b_2, Q)$ is the Sudakov factor in b space and S_t is the threshold resummation factor whose expressions can be found in [38,39] (we also list them in the Appendix),

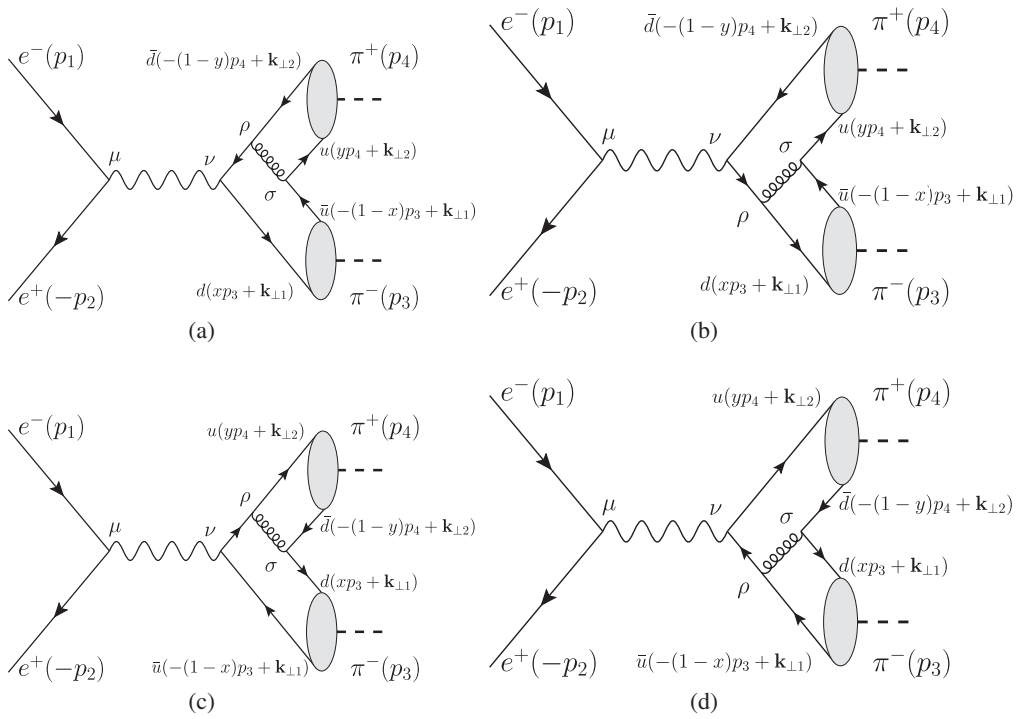

FIG. 2. Diagrams for $e^+e^- \to \pi^+\pi^-$ with OPE in the LO of pQCD.

$$T_H^{\nu,(a)} = c_f^{1\gamma}\mathrm{Tr}[\Phi_{\pi^+}^{(\mathrm{fin})}(p_4,y,\mathbf{k}_{\perp 2})(-ig_s\gamma^\sigma) \times \Phi_{\pi^-}^{(\mathrm{fin})}(p_3,x,\mathbf{k}_{\perp 1})\left(-\frac{1}{3}ie\gamma^\nu\right) \times S_q(q_q)(-ig_s\gamma^\rho)]D_{\rho\sigma}(q_g), \quad (5)$$

where $c_f^{1\gamma} = \frac{\delta_{ij}}{3}\frac{\delta_{mn}}{3}T^a_{jm}T^b_{ni}\delta_{ab} = \frac{4}{9}$ is the global color factor of the amplitude, g_s is the strong coupling, $-1/3$ is the charge of d-quark, $e = -|e|$ is the electromagnetic coupling, $S(q_q)$ and $D_{\rho\sigma}(q_g)$ are the propagators of the quark and gluon without the color indexes, q_q and q_g are the momenta of the corresponding quark and gluon in the propagators with

$$q_q \equiv [xp_3 + \mathbf{k}_{\perp 1}] - [p_3 + p_4],$$
$$q_g \equiv [yp_4 + \mathbf{k}_{\perp 2}] - [-(1-x)p_3 + \mathbf{k}_{\perp 1}], \quad (6)$$

and $\Phi_{\pi^\pm}^{(\mathrm{fin})}$ are the wave functions of $\pi^\pm$ expressed as

$$\Phi_{\pi^+}^{(\mathrm{fin})}(p_4,y,\mathbf{k}_{\perp 2}) = \frac{if_\pi}{4}\left\{\not{p}_4\gamma_5\phi_\pi(y) - \mu_\pi\gamma_5\left[\phi_\pi^P(y) - i\sigma_{\mu\nu} \times \left(\frac{p_4^\mu p_3^\nu}{p_4\cdot p_3}\frac{\phi_\pi^{\sigma\prime}(y)}{6} - p_4^\mu\frac{\phi_\pi^\sigma(y)}{6}\frac{\partial}{\partial\mathbf{k}_{\perp 2\nu}}\right)\right]\right\},$$
$$\Phi_{\pi^-}^{(\mathrm{fin})}(p_3,x,\mathbf{k}_{\perp 1}) = \frac{if_\pi}{4}\left\{\not{p}_3\gamma_5\phi_\pi(x) - \mu_\pi\gamma_5\left[\phi_\pi^P(x) - i\sigma_{\mu\nu} \times \left(\frac{p_3^\mu p_4^\nu}{p_3\cdot p_4}\frac{\phi_\pi^{\sigma\prime}(x)}{6} - p_3^\mu\frac{\phi_\pi^\sigma(x)}{6}\frac{\partial}{\partial\mathbf{k}_{\perp 1\nu}}\right)\right]\right\}, \quad (7)$$

with $f_\pi = 0.131$ GeV,

After including the contributions from the other diagrams and some algebraic calculation, the final expression for $F_\pi(Q^2)$ can be expressed as

$$F_\pi(Q^2) = \int_0^1 dxdy\int_0^\infty b_1db_1b_2db_2\alpha_s(\mu^2) \times e^{-S(x,y,b_1,b_2,Q)}S_t(x)\frac{16\pi f_\pi^2}{9} \times Q^2\left\{t_0 + \frac{\mu_\pi^2}{Q^2}[t_1+t_2+t_3]\right\}H_0^{(1)}(\sqrt{xy}Qb_2) \times [\theta(b_1-b_2)H_0^{(1)}(\sqrt{x}Qb_1)J_0(\sqrt{x}Qb_2) + \theta(b_2-b_1)H_0^{(1)}(\sqrt{x}Qb_2)J_0^{(1)}(\sqrt{x}Qb_1)], \quad (8)$$

where the scale μ in the coupling is taken as $\max\{\sqrt{x}Q, 1/b_1, 1/b_2\}$ and

$$t_0 = -\frac{1}{2}x\phi_\pi(y)\phi_\pi(x), \qquad t_1 = (1-x)\phi_\pi^P(y)\phi_\pi^P(x),$$
$$t_2 = -\frac{(1+x)}{6}\phi_\pi^P(y)\phi_\pi^T(x), \qquad t_3 = \frac{1}{3}\phi_\pi^P(y)\phi_\pi^\sigma(x). \quad (9)$$

Comparing Eqs. (8) and (9) with the expressions used in Refs. [30,31,34–36], two properties of Eq. (8) should be clarified. The first one is that Eq. (8) is consistent with the one in Ref. [30] in the spacelike region, and the factor $1/3$ in the term t_3 is different from the factor $1/2$ given in Ref. [31]. After some careful checking, we conclude this difference is due to the different deal on the term $\partial\not{k}_{\perp i}/\partial\mathbf{k}_{\perp i\mu}$. When one takes it as $\gamma_\perp^\mu$, one gets $1/3$, when one takes it as γ^μ one gets $1/2$. We take the factor $1/3$ in the final expression. In the practical numerical calculation, the contribution from this difference is very small in the spacelike region and usually neglected in some calculations, while it is not small in the timelike region and should be included. The second property of Eq. (8) is that there is a sign difference in the term t_2 between Eq. (8) and the one used in Ref. [34–36].

After some careful checking, we find the sign difference can be traced back to the definition of Eq. (7) and the corresponding Feynman diagrams in Fig. 2. After combining Eq. (7) and Fig. 2, one sees that the distribution of the u quark in π^+ is the same as the distribution of the d quark in π^-. This is right due to the isospin symmetry. In the practical calculation, this combination leads to the property that the four diagrams give the same expression $t_1 + t_2 + t_3$ except for some global factors. If one uses Eq. (7) and explains y as the distribution of the antiquark, then one can get $t_1 + t_2 + t_3$ for two diagrams and $t_1 - t_2 + t_3$ for another two diagrams. The correctness of Eq. (8) can also be verified via analytical continuation of the spacelike form factor to the timelike region. For example, if one applies the exchange $x \to 1-y$, $y \to 1-x$ to Eq. (8) of Ref. [30], uses the property $\phi_\pi(x) = \phi_\pi(1-x), \phi_\sigma(x) = \phi_\sigma(1-x), \phi_T(x) = -\phi_T(1-x)$, and does the analytical continuation for the Q^2, one finally gets the same results as our Eq. (8).

III. $e^+e^- \to \pi^+\pi^-$ VIA TWO-PHOTON-EXCHANGE

When the TPE contributions in the process $e^+e^- \to \pi^+\pi^-$ are considered, one has the corresponding diagrams shown in Fig. 3 in the LO.

The amplitude corresponding to Fig. 3(a) can be expressed as

$$i\mathcal{M}^{2\gamma,(a)} = \int dxdy\int d^2\mathbf{b}_1d^2\mathbf{b}_2\int\frac{d^2\mathbf{k}_{\perp 1}}{(2\pi)^2}\frac{d^2\mathbf{k}_{\perp 2}}{(2\pi)^2} \times e^{-i\mathbf{b}_1\cdot\mathbf{k}_{\perp 1}-i\mathbf{b}_2\cdot\mathbf{k}_{\perp 2}}e^{-S(x,y,b_1,b_2,Q)}T_H^{2\gamma,(a)} \triangleq \int K * T_H^{2\gamma,(a)}, \quad (10)$$

where

$$T_H^{2\gamma,(a)} = \bar{u}(-p_2,s_2)(-ie\gamma^\mu)S_e(q_e)(-ie\gamma^\rho)u(p_1,s_1) \times D_{\rho\sigma}(q_1)D_{\mu\nu}(q_2)c_{2\gamma}\mathrm{Tr}\left[\Phi_\pi^{(f)}(p_4,y,\mathbf{b}_2)\left(\frac{2}{3}ie\gamma^\nu\right) \times \Phi_{mn,\pi}^{(f)}(p_3,x,\mathbf{b}_1)\left(-\frac{1}{3}ie\gamma^\sigma\right)\right]$$
$$\triangleq \bar{u}(-p_2,s_2)\gamma^\mu\gamma^\omega\gamma^\rho u(p_1,s_1) \times q_{e,\omega}T_{\mu\rho}^{(a)}(Q^2,\theta,\mathbf{b}_1,\mathbf{k}_{\perp 1},\mathbf{b}_2,\mathbf{k}_{\perp 2}), \quad (11)$$

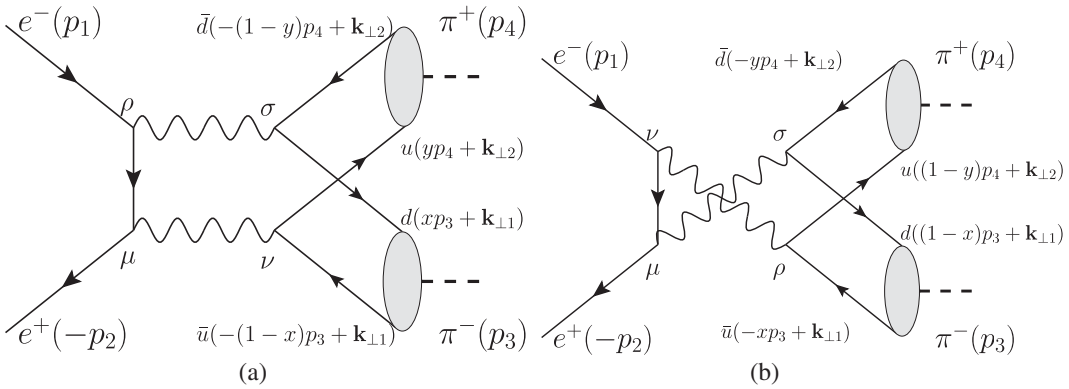

FIG. 3. Diagrams for TPE for $e^+e^- \to \pi^+\pi^-$ with two-photon exchange (TPE) in the LO of pQCD.

with $c_{2\gamma} = \frac{\delta_{ij}}{3}\frac{\delta_{ij}}{3} = \frac{1}{3}$ the global color factor and the momenta in the propagators

$$\begin{aligned} q_e &= -p_2 + q_2, \\ q_1 &= [xp_3 + \mathbf{k}_{\perp 1}] - [-(1-y)p_4 + \mathbf{k}_{\perp 2}], \\ q_2 &= [yp_4 + \mathbf{k}_{\perp 2}] - [-(1-x)p_3 + \mathbf{k}_{\perp 1}], \end{aligned} \tag{12}$$

and

$$\begin{aligned} &T^{(a)}_{\mu\rho}(Q^2, \theta, \mathbf{b}_1, \mathbf{k}_{\perp 1}, \mathbf{b}_2, \mathbf{k}_{\perp 2}) \\ &= c_{2\gamma}\mathrm{Tr}\left[\Phi_\pi(p_4, y, \mathbf{b}_2)\left(\frac{2}{3}ie\gamma_\mu\right)\Phi_\pi(p_3, x, \mathbf{b}_1)\right. \\ &\left.\times\left(-\frac{1}{3}ie\gamma_\rho\right)\right](-ie)^2\frac{-i}{q_1^2 + i\epsilon}\frac{-i}{q_2^2 + i\epsilon}\frac{i}{q_e^2 + i\epsilon}. \end{aligned} \tag{13}$$

The hard kernel $T_H^{2\gamma,(a)}$ is not gauge invariant itself, while the sum $T_H^{2\gamma,(a+b)}$ is gauge invariant. The check of the gauge invariance of the hard kernel $T_H^{2\gamma,(a+b)}$ is much simpler than that in the case of the next-to-leading-order contribution of the OPE amplitude, while it should also be verified carefully. In the practical calculation, one can separate the hard kernel as follows,

$$T_H^{2\gamma,(a+b)} \equiv L^{\mu\rho}D_{\rho\sigma}(q_1)D_{\mu\nu}(q_2)H_{\sigma\nu}, \tag{14}$$

with

$$\begin{aligned} L^{\mu\rho} &= \bar{u}(-p_2, s_2)(-ie\gamma^\mu)S_e(p_1 - q_1)(-ie\gamma^\rho)u(p_1, s_1) \\ &+ \bar{u}(-p_2, s_2)(-ie\gamma^\rho)S_e(p_1 - q_2)(-ie\gamma^\mu)u(p_1, s_1), \end{aligned} \tag{15}$$

where for simplicity we have exchanged the indexes of the lepton part in Fig. 3(b) to make sure the hadron parts of Figs. 3(a) and 3(b) are the same. The direct calculation shows

$$L^{\mu\rho}q_{1\rho} = 0, \qquad L^{\mu\rho}q_{2\mu} = 0. \tag{16}$$

These properties mean that the hard kernel $T_H^{2\gamma,(a+b)}$ is not dependent on the gauge parameter in the photon propagators $D_{\rho\sigma}(q_1)$ and $D_{\mu\nu}(q_2)$. This reflects that the result is not dependent on the choice of the gauge.

Using the relation

$$\gamma^\mu\gamma^\omega\gamma^\rho = g^{\mu\omega}\gamma^\rho - g^{\mu\rho}\gamma^\omega + g^{\omega\rho}\gamma^\mu - i\gamma^5\epsilon^{\mu\omega\rho\sigma}\gamma_\sigma, \tag{17}$$

the amplitude $i\mathcal{M}^{2\gamma,(a)}$ can be expressed in a similar form as $i\mathcal{M}^{1\gamma}$ and one has

$$\begin{aligned} T_H^{2\gamma,(a)}(p_1, s_1; p_2, s_2; p_3, p_4) &= \bar{u}(-p_2, s_2)\gamma^\rho u(p_1, s_1)q_{e,\omega}T^{(a)}_{\omega\rho} - \bar{u}(-p_2, s_2)\gamma^\omega u(p_1, s_1)q_{e,\omega}T^{(a)}_{\mu\mu} \\ &+ \bar{u}(-p_2, s_2)\gamma^\mu u(p_1, s_1)q_{e,\rho}T^{(a)}_{\mu\rho} - \bar{u}(-p_2, s_2)\gamma^\sigma u(p_1, s_1)i\gamma_5\epsilon^{\mu\omega\rho}{}_\sigma q_{e,\omega}T^{(a)}_{\mu\rho}) \\ &= [\bar{u}(-p_2, m_e)\gamma^\mu u(p_1, m_e)][q_{e,\omega}T^{(a)}_{\omega\mu} - q_{e,\mu}T^{(a)}_{\rho\rho} + q_{e,\rho}T^{(a)}_{\mu\rho}] \\ &+ [\bar{u}(-p_2, m_e)\gamma_5\gamma^\mu u(p_1, m_e)][-i\epsilon^{\sigma\omega\rho}{}_\mu q_{e,\omega}T^{(a)}_{\sigma\rho}], \\ &\triangleq [\bar{u}(-p_2, m_e)(-ie\gamma_\mu)u(p_1, m_e)]D^{\mu\nu}(q)T^{(a),\mathrm{eff}}_\nu \\ &+ [\bar{u}(-p_2, m_e)(-ie\gamma_5\gamma_\mu)u(p_1, m_e)]D^{\mu\nu}(q)\bar{T}^{(a),\mathrm{eff}}_\nu, \end{aligned} \tag{18}$$

with

$$T_\nu^{(a),\mathrm{eff}} = \frac{1}{-ie}\frac{q^2}{-i}[q_{e,\omega}T^{(a)}_{\omega\nu} - q_{e,\nu}T^{(a)}_{\rho\rho} + q_{e,\rho}T^{(a)}_{\nu\rho}],$$
$$\bar{T}_\nu^{(a),\mathrm{eff}} = \frac{1}{-ie}\frac{q^2}{-i}[-i\epsilon^{\sigma\omega\rho}{}_\nu q_{e,\omega}T^{(a)}_{\sigma\rho}]. \tag{19}$$

Generally, $T_\nu^{(a),eff}$ can be written as $c_1 p_{1\nu} + c_2 p_{2\nu} + c_3 p_{3\nu}$. Using the approximation $m_e = 0$, the first two terms give no contributions and one gets $T_\nu^{(a),\mathrm{eff}} \propto (p_4 - p_3)_\nu$ and finally

$$\begin{aligned} i\mathcal{M}^{2\gamma,(a)} &= \int K * [\bar{u}(-p_2, m_e)(-ie\gamma_\mu)u(p_1, m_e)]D^{\mu\nu}(q)T_\nu^{\mathrm{eff}}] \\ &\quad + \int K * [\bar{u}(-p_2, m_e)(-ie\gamma_5\gamma_\mu)u(p_1, m_e)]D^{\mu\nu}(q)\tilde{T}_\nu^{\mathrm{eff},(a)}] \\ &\triangleq [\bar{u}(-p_2, m_e)(-ie\gamma_\mu)u(p_1, m_e)]D^{\mu\nu}(q)[-ie(p_4 - p_3)_\nu \tilde{F}_\pi^{(a)}(Q^2, \theta)], \\ &\quad + [\bar{u}(-p_2, m_e)(-ie\gamma_5\gamma_\mu)u(p_1, m_e)]D^{\mu\nu}(q)[-ie(p_4 - p_3)_\nu \tilde{G}_\pi^{(a)}(Q^2, \theta)], \end{aligned} \tag{20}$$

where $\tilde{F}_\pi(Q^2, \theta), \tilde{G}_\pi(Q^2, \theta)$ are expressed as

$$\tilde{F}_\pi^{(a)}(Q^2, \theta) = \int \frac{(p_4 - p_3)^\nu}{-ie(p_4 - p_3)^2} T_\nu^{(a),\mathrm{eff}},$$
$$\tilde{G}_\pi^{(a)}(Q^2, \theta) = \int \frac{(p_4 - p_3)^\nu}{-ie(p_4 - p_3)^2} \bar{T}_\nu^{(a),\mathrm{eff}}. \tag{21}$$

The contribution from Fig. 3(b) can de found in a similar way. Due to the similar form with $F_\pi(Q^2)$, we call $\tilde{F}_\pi^{(a)}(Q^2, \theta), \tilde{G}_\pi^{(a)}(Q^2, \theta)$ the general form factors in the following and the final expressions for the general form factors can be derived from Eqs. (13), (19), and (21).

After some calculation, one has

$$\begin{aligned} \tilde{F}_\pi(Q^2, \theta) &\triangleq \tilde{F}_\pi^{(a)}(Q^2, \theta) + \tilde{F}_\pi^{(b)}(Q^2, \theta), \\ \tilde{F}_\pi^{(b)}(Q^2, \theta) &= -\tilde{F}_\pi^{(a)}(Q^2, \theta + \pi), \end{aligned} \tag{22}$$

where

$$\begin{aligned} \tilde{F}_\pi^{(a)}(Q^2, \theta) &= \frac{c_{2\gamma}e^2 f_\pi^2 Q^2}{36\pi}\int b_2 db_2 \int dxdy e^{-S(x,y,b_1,b_2,Q)} \\ &\times \left\{\frac{1}{2}\phi_\pi(x)\phi_\pi(y)Q^2(-\cos\theta + x + y - 1) + \mu_\pi^2[\phi_\pi^P(x)\phi_\pi^P(y)(-\cos\theta + x + y - 1)\right. \\ &\left. -\frac{1}{36}\phi_\pi^T(x)\phi_\pi^T(y)(-\cos\theta + x + y - 1) + \frac{1}{24}\phi_\pi^T(x)\phi_\pi^\sigma(y) + \frac{1}{24}\phi_\pi^\sigma(x)\phi_\pi^T(y)]\right\}\tilde{H}(x, y, Q, b_2, \theta), \end{aligned} \tag{23}$$

and

$$\begin{aligned} \tilde{H}(x, y, Q, b_2, \theta) = \int d\phi_{b_2} dk_{\perp 3x} e^{-ib_{2x}k_{\perp 3x}} \Bigg\{ & \frac{2\sqrt{2}e^{\frac{|b_{2y}|}{\sqrt{2}}\left(-\sqrt{P_1^{(1)}(x,y,Q,k_{\perp 3x},\theta)-i\epsilon}\right)}}{\sqrt{P_1^{(1)}(x, y, Q, k_{\perp 3x}, \theta) - i\epsilon}P_2^{(1)}(x, y, Q, k_{\perp 3x}, \theta)P_3^{(1)}(x, y, Q, k_{\perp 3x}, \theta)} \\ & - \frac{e^{|b_{2y}|\left(-\sqrt{P_1^{(2)}(x,y,Q,k_{\perp 3x})-i\epsilon}\right)}}{\sqrt{P_1^{(2)}(x, y, Q, k_{\perp 3x}) - i\epsilon}P_2^{(2)}(x, y, Q)P_3^{(2)}(x, y, Q, k_{\perp 3x}, \theta)} \\ & + \frac{e^{|b_{2y}|\left(-\sqrt{P_1^{(3)}(x,y,Q,k_{\perp 3x})-i\epsilon}\right)}}{\sqrt{P_1^{(3)}(x, y, Q, k_{\perp 3x}) - i\epsilon}P_2^{(3)}(x, y, Q)P_3^{(3)}(x, y, Q, k_{\perp 3x}, \theta)} \Bigg\}, \end{aligned} \tag{24}$$

with $b_{2y} \triangleq b_2 \sin\phi_{b_2}$, $b_{2x} \triangleq b_2 \cos\phi_{b_2}$, $k_{\perp 3} = k_{\perp 2} - k_{\perp 1} = \{k_{\perp 3x}, k_{\perp 3y}\}$, $\epsilon = 0^+$ and

$$\begin{aligned}
P_1^{(1)}(x,y,Q,k_{\perp 3x},\theta) &= 2k_{\perp 3x}^2 + 2k_{\perp 3x}Q\sin\theta + Q^2(-\cos\theta(x+y-1) + 2xy - x - y + 1) + 2m_e^2,\\
P_2^{(1)}(x,y,Q,k_{\perp 3x},\theta) &= 2k_{\perp 3x}Q\sin\theta + Q^2(-\cos\theta(x+y-1) + x - y + 1) + 2m_e^2,\\
P_3^{(1)}(x,y,Q,k_{\perp 3x},\theta) &= 2k_{\perp 3x}Q\sin\theta + Q^2(-\cos\theta(x+y-1) - x + y + 1) + 2m_e^2,\\
P_1^{(2)}(x,y,Q,k_{\perp 3x}) &= k_{\perp 3x}^2 + Q^2(x-1)y,\\
P_2^{(2)}(x,y,Q) &= Q^2(x-y),\\
P_3^{(2)}(x,y,Q,k_{\perp 3x},\theta) &= P_3^{(1)}(x,y,Q,k_{\perp 3x},\theta),\\
P_1^{(3)}(x,y,Q,k_{\perp 3x}) &= k_{\perp 3x}^2 + Q^2 x(y-1),\\
P_2^{(3)}(x,y,Q) &= P_2^{(2)}(x,y,Q),\\
P_3^{(3)}(x,y,Q,k_{\perp 3x},\theta) &= P_2^{(1)}(x,y,Q,k_{\perp 3x},\theta).
\end{aligned} \tag{25}$$

From Eq. (25), one can see that there are some singularities in the integrated kernel, and these singularities are located at $x = y$ or the end points with $k_T = 0$. In the practical calculation, the contributions of these singularities are suppressed by the behavior of the corresponding Sudkov factors, and the final results are safe without any divergence.

Furthermore, the cross section from the interference of $\mathcal{M}^{2\gamma}$ and $\mathcal{M}^{1\gamma}$ can expressed as

$$d\sigma_{un}^{2\gamma} = \frac{1}{2}e^2\sin^2\theta\{2\mathrm{Re}[F_\pi^*(Q^2)\tilde{F}_\pi(Q^2,\theta)]\}, \tag{26}$$

and there is no contribution from $\tilde{G}_\pi(Q^2,\theta)$.

IV. THE INPUT

In the timelike region, in principle, the contributions from the resonances should also be considered. In this work, we limit our discussion to the high-energy region and focus on the TPE effects, so we neglect the contributions from the resonances at present, and the needed inputs are the same as those used in the spacelike region. For simplicity, we directly take $n_f = 3, \Lambda = 0.2$ GeV in the Sudakov factor and neglect the dependence of n_f and Λ on Q^2, $1/b_1$, and $1/b_2$. All other inputs are taken as the same as those used in Ref. [35] which means the asymptotic two-parton twist-2 and twist-3 DAs are taken as

$$\begin{aligned}
\phi_\pi(x) &= 6x(1-x)[1 + a_2 C_2^{3/2}(1-2x)],\\
\phi_\pi^P(x) &= 1,\\
\phi_\pi^\sigma(x) &= 6x(1-x),\\
\phi_\pi^T(x) &= d\phi_\pi^\sigma(x)/dx = 6(1-2x),
\end{aligned} \tag{27}$$

with $a_2 = 0.2$ and the Gegenbauer polynomial $C_2^{3/2}(u) = (3/2)(5u^2 - 1)$. The normalization of the above DAs is a little different from that in Ref. [35]. The associated chiral scale is taken as $\mu_\pi = 1.3$ GeV, the shape parameter in the threshold resummation factor $S_t(x)$ is taken as $c = 0.4$, and the renormalization scale used in the α_S and Sudakov factor is taken as $\mu = \max(\sqrt{x}Q, 1/b_1, 1/b_2)$.

Other forms of DAs are also used for estimation and the practical numerical results show the form factors are a little sensitive on the input DAs. Since our focus is on the TPE effects in $e^+e^- \to \pi^+\pi^-$, we do not discuss the details of the dependence of the pion form factor $Q^2|F_\pi(Q^2)|$ on the input DAs.

V. NUMERICAL RESULTS AND DISCUSSION

Using the inputs suggested in the last section, the form factors $F_\pi(Q^2), \tilde{F}_\pi(Q^2,\theta)$ can be calculated directly by the numerical method. In our numerical calculation, we use the NIntegrate function in MATHEMATICA to do the integration and also the Bessel function. The Vegas function in the package CUBA [40] is also used to check the numerical calculation, and we find it gives the same results. We want to point out that the integration that includes the Bessel function should be dealt with carefully. The integration of $Q^2|\tilde{F}_\pi(Q^2,\theta)|$ is heavy, and in the practical calculation, we at first calculate the results at some points with the relative precision about 1% and then fit the results.

The numerical results for $Q^2|F_\pi(Q^2)|$ and the phase of $F_\pi(Q^2)$ are presented in Fig. 4. The red dashed curves refer to the contribution from twist-2 DA, the blue dotted curves refer to the contribution from twist-3 DAs, the black solid curves refer to the contribution from their sum and the Ex-data sets are taken from Ref. [41]. The contribution from the twist-2 DA is almost same with that presented in [35]. The contribution from the twist-3 DAs is much smaller than that from the twist-2 DA, which is very different from the property presented in [35,36]. This property leads to the full

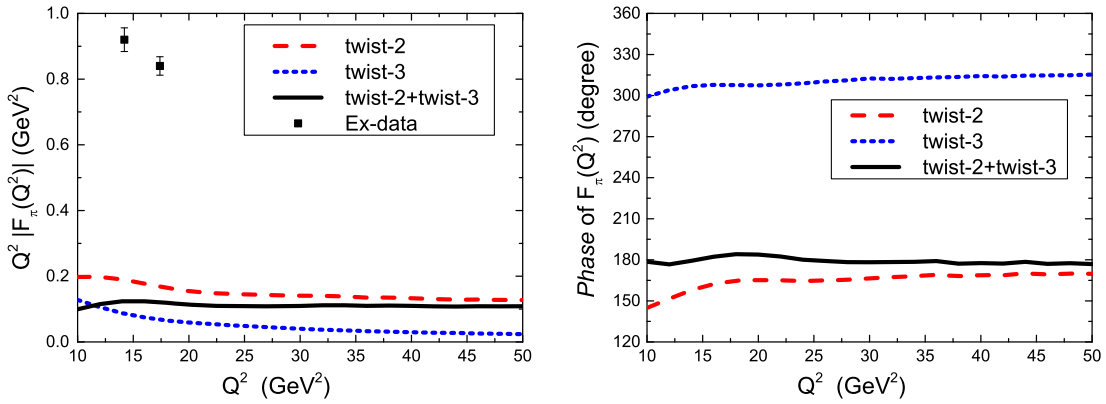

FIG. 4. Results for $Q^2F_\pi(Q^2)$ *vs* Q^2. The left panel is the result for $Q^2|F_\pi(Q^2)|$ *vs* Q^2 and the right panel is the result for the phase of $F_\pi(Q^2)$ *vs* Q^2. The red dashed curves refer to the contribution from twist-2 DA, the blue dotted curves refer to the contribution from twist-3 DAs, the black solid curves refer to the contribution from their sum, and the Ex-data sets are taken from Ref. [41].

results in the LO of pQCD are much smaller than the experimental data at $Q^2 = 14.2$, 17.4 GeV^2. For comparison, three results are presented in Fig. 5 to show the reason for the large difference.

In Fig. 5, the olive dashed curves labeled as "twist-3-refs" refer to the results by replacing $t_1 + t_2 + t_3$ in Eq. (8) with $t_1 - t_2$ which was given in [34] and then used in Refs. [35,36], the pink dashed-doted curves labeled as "twist-3-corrected" refer to the results by replacing $t_1 + t_2 + t_3$ in Eq. (8) with $t_1 + t_2$, and the black solid curves labeled as "twist-3-full" refer to the results from Eq. (8). The numerical results "twist-3-Refs" are almost the same as the corresponding results in Fig. 5 of Ref. [35]. The comparison of the results "twist-3-refs" and "twist-3-corrected" shows that there is large cancellation between the contributions from the terms t_1 and t_2. The comparison of the results "twist-3-corrected" and "twist-3-full" shows the contribution from the term t_3 is also important. The property of the contribution from the term t_3 is very different from that in the spacelike region where the contribution from this term is small.

From the numerical results of Figs. 4 and 5, one can see that the results in the LO of pQCD are incomplete to explain the current experimental data at $Q^2 = 14.2$, 17.4 GeV^2 which are located at the masses of the resonances $\psi(3770)$ and $\psi(4160)$. This is natural since, in these regions, the contributions from the resonances play important roles due to their strong coupling with the pion pair and should be considered in a nonperturbative way. The pQCD results are expected to be good only when Q^2 is large enough and far away from these resonances. This conclusion is very different from that given by Refs. [35,36], and the main reason is due to the sign difference in Eq. (8).

The numerical results for $Q^2|\tilde{F}_\pi(Q^2,\theta)|$ *vs* Q^2 at $\theta = (1/9, 2/9, 1/3, 4/9)\pi$ are presented in Fig. 6. The red dashed curves refer to the contribution from twist-2 DA, the blue dotted curves refer to the contribution from twist-3 DAs, and the black solid curves refer to the contribution from their sum. One can see the magnitudes of $Q^2|\tilde{F}_\pi(Q^2,\theta)|$ are about (10%–20%) of $Q^2|F_\pi(Q^2)|$ at small θ, which

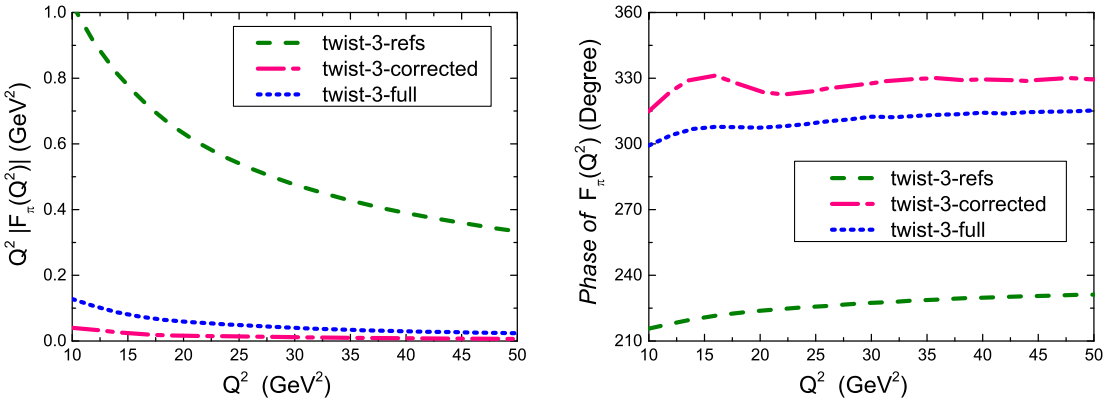

FIG. 5. Comparison of the contributions from twist-3 DAs to $Q^2|F_\pi(Q^2)|$ and the phase of $F_\pi(Q^2)$ with different expressions. The olive dashed curves labelled as "twist-3-refs" refers to the results by replacing $t_1 + t_2 + t_3$ in Eq. (8) with $t_1 - t_2$ which was given in [34] and then used in Refs. [35,36], the pink dashed-doted curves labeled as "twist-3-corrected" refers to the results by replacing $t_1 + t_2 + t_3$ in Eq. (8) with $t_1 + t_2$ and the black solid curves labeled as "twist-3-full" refers to the results by Eq. (8).

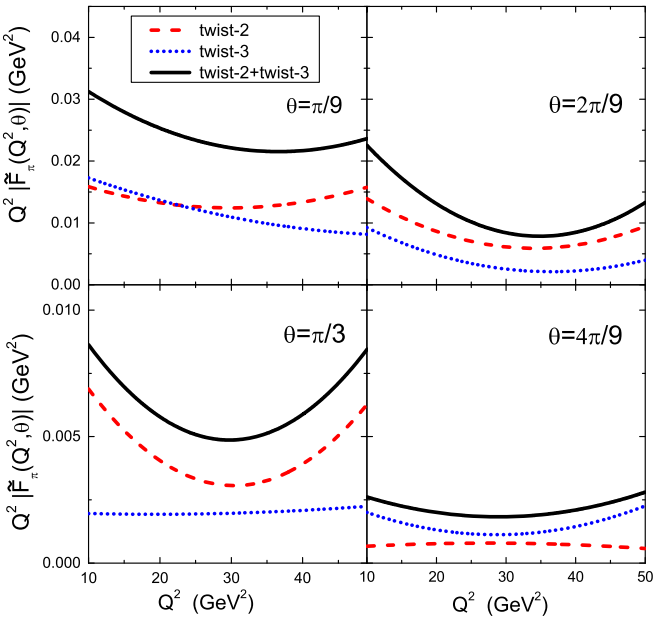

FIG. 6. The numerical results for $Q^2|\tilde{F}_\pi(Q^2,\theta)|$ *vs* Q^2 at $\theta = (1/9, 2/9, 1/3, 4/9)\pi$ from twist-2 DA (red dashed), twist-3 DAs (blue dotted), and their sum (black solid), respectively.

means the absolute contributions from the TPE effects are not small. This is natural since naively the ratio is expected as $\alpha_{\rm QED}/\alpha_S$ due to Figs. 2 and 3. This property is different from the TPE corrections in the elastic ep scattering at small momentum transfer where the relative corrections are expected as $\alpha_{\rm QED}$. The $Q^2|\tilde{F}_\pi(Q^2,\theta)|$ also shows strong angle dependence which is the most interesting property difference from $F_\pi(Q^2)$. The manifest dependence of $Q^2|\tilde{F}_\pi(Q^2,\theta)|$ on θ at $Q^2 = (20, 50)$ GeV^2 is presented in Fig. 7.

The normalized cross sections $d\sigma_{un}Q^4/\sin^2\theta$ from the OPE (black solid curves) and OPE + TPE (red dashed curves) are presented in Fig. 8, where one can see a manifest asymmetry in the angle dependence of the cross section after including the TPE effects. The existence of such asymmetry is a direct single of the TPE effects. The measurements of such asymmetry can help us understand the TPE effects.

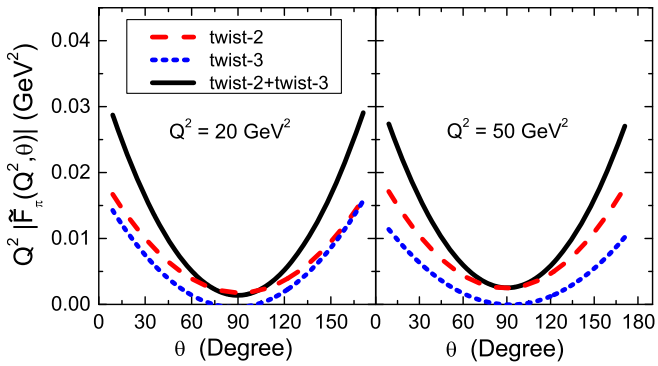

FIG. 7. The numerical results for $Q^2|\tilde{F}_\pi(Q^2,\theta)|$ *vs* θ at $Q^2 = (20, 50)$ GeV^2 from twist-2 DA (red dashed), twist-3 DA (blue dotted), and their sum (black solid), respectively.

In summary, in this work, the TPE effects in the process $e^+e^- \to \pi^+\pi^-$ at large momentum transfer are discussed within the pQCD. The TPE contributions to the cross section are calculated, and we find the asymmetry of the differential cross section on the scattering angle reaches about 10%–20% at small angle. The timelike electromagnetic form factor of the pion at the LO of α_S from the twist-3 DAs is also discussed, and the comparison of our results with those in the references is presented. Our results show the contributions from the twist-2 and twist-3 DAs in the LO of pQCD are much smaller than the experimental data at $Q^2 = 14.2,\ 17.4$ GeV^2, which is very different from the conclusion given in the Refs. [35,36].

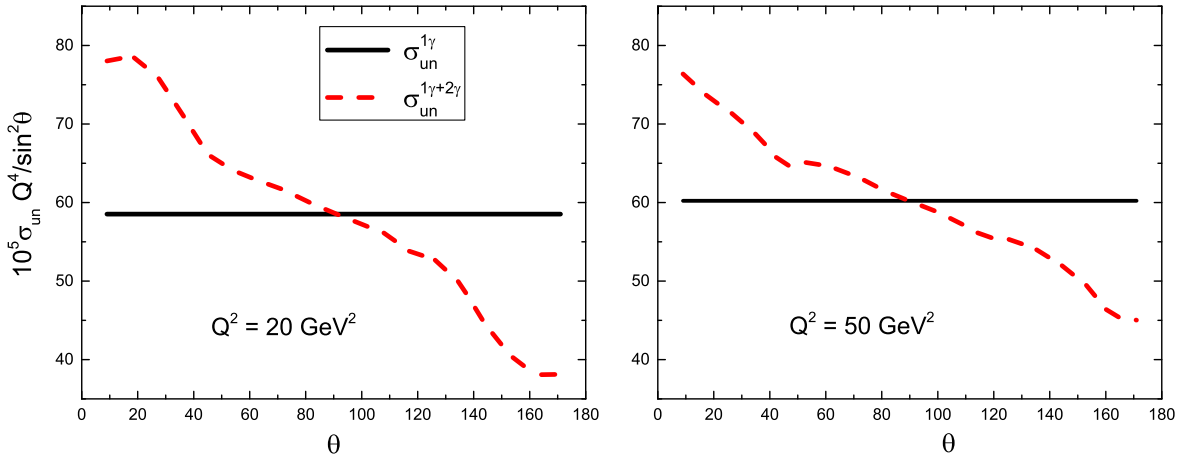

FIG. 8. The numerical results for $d\sigma_{un}Q^4/\sin^2\theta$ *vs* θ at $Q^2 = (20, 50)$ GeV^2 from the OPE (black solid) and OPE + TPE (red dashed), respectively.

ACKNOWLEDGMENTS

H.-Q. Zhou would like to thank Hsiang-nan Li, Xing-Gang Wu, and Shan Cheng for their kind and helpful discussions. This work is supported by the National Natural Science Foundations of China under Grant No. 11375044.

APPENDIX: SOME BASIC EXPRESSIONS

In this Appendix, some expressions used in the practical calculation are listed.

The Sudkov factor $S(x, y, b_1, b_2, Q)$ [38] is expressed as

$$S(x,y,b_1,b_2,Q) = s(xQ,b_1) + s(yQ,b_2) + s((1-x)Q,b_1) + s((1-y)Q,b_2) - \frac{1}{\beta_0}\ln\left(\frac{\hat{t}}{-\hat{b}_1}\right) - \frac{1}{\beta_0}\ln\left(\frac{\hat{t}}{-\hat{b}_2}\right), \quad \text{(A1)}$$

where

$$s(xQ,1/b) = \frac{A^{(1)}}{2\beta_0}\hat{q}\ln\left(\frac{\hat{q}}{-\hat{b}}\right) + \frac{A^{(2)}}{4\beta_0^2}\left(\frac{\hat{q}}{-\hat{b}} - 1\right) - \frac{A^{(1)}}{2\beta_0}(\hat{b}+\hat{q}) - \frac{4A^{(1)}\beta_1}{16\beta_0^3}\hat{q}\left[\frac{1+\ln(-2\hat{b})}{-\hat{b}} - \frac{1+\ln(2\hat{q})}{\hat{q}}\right] - \left[\frac{A^{(2)}}{4\beta_0^2} - \frac{A^{(1)}}{4\beta_0}\ln\left(\frac{1}{2}e^{2\gamma_E-1}\right)\right]\ln\left(\frac{\hat{q}}{-\hat{b}}\right) - \frac{4A^{(1)}\beta_1}{32\beta_0^3}[\ln^2(-2\hat{b}) - \ln^2(2\hat{q})], \quad \text{(A2)}$$

with

$$\hat{t} = \ln\left(\frac{t}{\Lambda_{\rm QCD}}\right), \qquad t = \max(\sqrt{x}Q, 1/b_1, 1/b_2),$$
$$\hat{b} = \ln(b\Lambda_{\rm QCD}), \qquad \hat{q} = \ln\left[\frac{xQ}{\sqrt{2}\Lambda_{\rm QCD}}\right],$$
$$A^{(1)} = C_F = \frac{4}{3},$$
$$A^{(2)} = \left(\frac{67}{27} - \frac{\pi^2}{9}\right)N_c - \frac{10}{27}N_f + \frac{8}{3}\beta_0\ln\left(\frac{e^{\gamma_E}}{2}\right),$$
$$\beta_0 = \frac{11N_c - 2N_f}{12} = \frac{9}{4}, \qquad \beta_1 = \frac{51N_c - 19N_f}{24} = 4,$$
$$N_c = N_f = 3. \quad \text{(A3)}$$

The jet function $S_t(x_i)$ [39] is expressed as

$$S_t(x_i) = \frac{2^{1+2c}\Gamma(3/2+c)}{\sqrt{\pi}\Gamma(1+c)}[x_i(1-x_i)]^c. \quad \text{(A4)}$$

The running strong coupling α_S [42] is expressed as

$$\alpha_s(\mu^2) = \frac{\pi}{\beta_0\ln(\mu^2/\Lambda^2_{\rm QCD})} - \frac{\pi\beta_1\ln(\ln(\mu^2/\Lambda^2_{\rm QCD}))}{\beta_0^3\ln^2(\mu^2/\Lambda^2_{\rm QCD})}. \quad \text{(A5)}$$

[1] M. K. Jones *et al.* (JLab Hall A Collaboration), Phys. Rev. Lett. **84**, 1398 (2000).
[2] O. Gayou *et al.* (JLab Hall A Collaboration), Phys. Rev. Lett. **88**, 092301 (2002).
[3] L. Andivahis *et al.*, Phys. Rev. D **50**, 5491 (1994).
[4] R. C. Walker *et al.*, Phys. Rev. D **49**, 5671 (1994).
[5] P. G. Blunden, W. Melnitchuk, and J. A. Tjon, Phys. Rev. Lett. **91**, 142304 (2003).
[6] S. Kondratyuk, P. G. Blunden, W. Melnitchuk, and J. A. Tjon, Phys. Rev. Lett. **95**, 172503 (2005).
[7] P. G. Blunden, W. Melnitchuk, and J. A. Tjon, Phys. Rev. C **72**, 034612 (2005).
[8] H.-Y. Chen and H.-Q. Zhou, Phys. Rev. C **90**, 045205 (2014).
[9] Y. C. Chen, A. Afanasev, S. J. Brodsky, C. E. Carlson, and M. Vanderhaeghen, Phys. Rev. Lett. **93**, 122301. (2004).
[10] A. Afanasev, S. J. Brodsky, C. E. Carlson, Y. C. Chen, and M. Vanderhaeghen, Phys. Rev. D **72**, 013008 (2005).
[11] Y. C. Chen, C. W. Kao, and S. N. Yang, Phys. Lett. B **652**, 269 (2007).
[12] D. Borisyuk and A. Kobushkin, Phys. Rev. C **76**, 022201 (2007).
[13] D. Borisyuk and A. Kobushkin, Phys. Rev. C **78**, 025208 (2008).
[14] D. Borisyuk and A. Kobushkin, Phys. Rev. C **74**, 065203 (2006).
[15] D. Borisyuk and A. Kobushkin, Phys. Rev. C **83**, 025203 (2011).
[16] D. Borisyuk and A. Kobushkin, Phys. Rev. C **86**, 055204 (2012).
[17] D. Borisyuk and A. Kobushkin, Phys. Rev. C **89**, 025204 (2014).
[18] P. G. Blunden and W. Melnitchouk, Phys. Rev. C **95**, 065209 (2017).
[19] D. Borisyuk and A. Kobushkin, Phys. Rev. C **79**, 034001 (2009).

[20] N. Kivel and M. Vanderhaeghen, Phys. Rev. Lett. **103**, 092004 (2009).
[21] N. Kivel and M. Vanderhaeghen, J. High Energy Phys. 04 (2013) 029.
[22] B. S. Henderson, Phys. Rev. Lett. **118**, 092501 (2017).
[23] D. Y. Chen, H. Q. Zhou, and Y. B. Dong, Phys. Rev. C **78**, 045208 (2008).
[24] P. G. Blunden, W. Melnitchouk, and J. A. Tjon, Phys. Rev. C **81**, 018202 (2010).
[25] Y. B. Dong and S. D. Wang, Phys. Lett. B **684**, 123 (2010).
[26] D.-Y. Chen and Y.-B. Dong, Phys. Rev. C **87**, 045209 (2013).
[27] O. Tomalak and M. Vanderhaeghen, Phys. Rev. D **90**, 013006 (2014).
[28] O. Koshchii and A. Afanasev, Phys. Rev. D **94**, 116007 (2016).
[29] H.-Q. Zhou, Phys. Rev. C **95**, 025203 (2017).
[30] Z.-T. Wei and M.-Z. Yang, Phys. Rev. D **67**, 094013 (2003).
[31] T. Huang and X.-G. Wu, Phys. Rev. D **70**, 093013 (2004).
[32] U. Raha and A. Aste, Phys. Rev. D **79**, 034015 (2009).
[33] T. Gousset and B. Pire, Phys. Rev. D **51**, 15 (1995).
[34] J. W. Chen, H. Kohyama, K. Ohnishi, U. Raha, and Y.-L. Shen, Phys. Lett. B **693**, 102 (2010).
[35] H.-C. Hu and H.-n. Li, Phys. Lett. B **718**, 1351 (2013).
[36] S. Cheng and Z.-J. Xiao, Phys. Lett. B **749**, 1 (2015).
[37] G. P. Lepage and S. J. Brodsky, Phys. Rev. Lett. **43**, 545 (1979); G. P. Lepage and S. J. Brodsky, Phys. Rev. D **22**, 2157 (1980); J. Botts and G. Sterman, Nucl. Phys. **B325**, 62 (1989); H-n. Li and G. Sterman, Nucl. Phys. **B381**, 129 (1992).
[38] J. Botts and G. Sterman, Nucl. Phys. **B325**, 62 (1989); H.-N. Li and G. Sterman, Nucl. Phys. **B381**, 129 (1992).
[39] T. Kurimoto, H. N. Li, and A. I. Sanda, Phys. Rev. D **65**, 014007 (2001); H. N. Li, Phys. Rev. D **66**, 094010 (2002).
[40] T. Hahn, Comput. Phys. Commun. **168**, 78 (2005); **207**, 341 (2016).
[41] K. K. Seth, S. Dobbs, Z. Metreveli, A. Tomaradze, T. Xiao, and G. Bonvicini, Phys. Rev. Lett. **110**, 022002 (2013).
[42] Particle Data Group, Chin. Phys. C **40**, 100001 (2016).